V European Conference on Computational Fluid Dynamics
ECCOMAS CFD 2010
J. C. F. Pereira and A. Sequeira (Eds)
Lisbon, Portugal,14-17 June 2010

DOWNSCALING A LARGE-SCALE OCEAN-BASIN MODEL: AN INTERCOMPARISON EXERCISE IN THE BAY OF BISCAY

Guillaume Riflet[†], Guillaume Reffray[*], Rodrigo Fernandes[†], Paulo Chambel[‡], João Nogueira[†], Ramiro Neves[†]

[†]Instituto Superior Técnico, Universidade Técnica de Lisboa
Av. Rovisco Pais 1, 1049-001 Lisboa, Portugal
e-mail: guillaume.maretec@ist.utl.pt
[*]Mercator-Océan
8/10 rue Hermès, 31520 Ramonville St-Agne, France
[‡]Hidromod consulting
Av. Manuel da Maia, nº 36, 3º esq. 1000-201 Lisboa, Portugal

Key words: Bay of Biscay, Regional Ocean modeling, Boundary conditions, Model intercomparison

Abstract. *To provide good open boundary conditions to local numerical models, a nesting approach is often undertaken in which the local model is nested into a coastal model, which in turn is nested into an ocean basin model. MOHID is known to be an estuarine model [4, 15, 25] which has the capacity as well of modeling the physical processes at the coastal scale [22, 12]. The inherent challenge consists in integrating data from different models at different scales and to assess the quality of the nested solution. This work consists in assessing the skill of MOHID to actuate as a coastal model, nested offline into an ocean-basin solution, by implementing it to the Bay of Biscay. A generic nesting methodology is proposed. The results are then compared with a climatology, in-situ data and remote-sensed data. An intercomparison with another model that run during the same period with the same forcing is also made. The results show that MOHID is capable to produce a realistic solution that is well comparable with other state-of-the-art numerical models.*

1 INTRODUCTION

Regional Ocean models are often used in regional, coastal, as well as operational oceanography. They are numerical models that implement the primitive Ocean equations (the mathematical standard model to describe geophysical fluids), and apply them to a region of the Ocean, usually containing a coastline, a continental-shelf, a continental slope and an abyssal plain. The numerical models are of great use for scientists and engineers to assess and infer Oceanographical knowledge from hydrographical field-data. These studies can help to better understand the Ocean, making predictions to Ocean conditions and even help to assist fisheries and coastal management at an ecological, economical and political level.

However, when modeling a region of the Ocean there are several important issues that the modeler must face. One is having an adequate state-of-art numerical model, with a proven record of regional Ocean modeling capability. Another issue is having adequate forcings and initial conditions (IC) for the region of the Ocean. Yet another issue is to have in-situ data for validation of the model's results. A final issue is to choose consistent open-boundary conditions (OBC).

This work proposes to address the first and the last issue, by describing and proposing an inter-comparison exercise for the Ocean region of the bay of Biscay for the full year of 2004, consisting of the validation and comparison of two models, each implementing its OBC, but using exactly the same forcings and the same IC. Hence, this work main objectives are to assess the regional Ocean modeling capabilities of tested regional Ocean models and to propose a state-of-the-art downscaling methodology.

The added interest is that IC, in-situ and remote-sensing data were gathered and a suite of tests was devised. This data is freely available (upon request to the authors) so that any regional Ocean modeling system can reproduce the yearly run and compare directly its results with those exposed in this work. It is expected that more modelers compare their results with the results exposed in this work, eventually extending them and improving them. Such inter-comparison exercises, due to the heavy collaboration between institutes and research teams, are found only quite scarcely in the literature [24].

For this regional Ocean modeling exercise, the bay of Biscay was chosen, where in-situ data from two cruise campaigns EVHOE and PELGAS were made available and remote-sensing data from MODIS was used. Also, a climatology provided by IFREMER is made available for further reference. The IC and OBC reference solution is the ocean general circulation model (OGCM) PSY2V1 solution of the North-Atlantic, provided by Mercator-Océan. The surface forcing is ensured by the atmospheric model ALADDIN. The bathymetry (bottom forcing) is provided by ETOPO data. Two models were run, each with their own experimental parameterization introduced by independent teams, NEMO-OPA and MOHID.

The layout of the work is as follows: first the general circulation and the oceanographic features of the Ocean region of the bay of Biscay are described. Then, a listing of the

available data for validation and comparison is described. Later on, a brief description of the numerical models, NEMO-OPA and MOHID is made. The experimental setup and forcing data is also described. Finally, the analysis of the results and the comparison is made in the last section.

2 CIRCULATION, PROCESSES AND FIELD DATA IN THE BAY OF BISCAY

2.1 The Bay of Biscay in the North Atlantic Ocean

The Atlantic general circulation of the northern hemisphere consists in the anti-cyclonic sub-tropical gyre, intensified on the American continent coast (the Gulf Stream: intense surface and warm current), and the sub-polar cyclonic gyre, separated roughly at the latitude of 45°N. The Gulf Stream branches at about 42°N. One of the branches derives south-eastward, crosses the Atlantic ridge, south of the Azores archipelago (between 32°N and 37°N) and enters the eastern basin thus forming the Azores Current (AzC). The other branch moves north-eastward, forming the North-Atlantic Drift (NAD). At the level of the Charlie-Gibbs fracture situated at 52°N and 26°W, a NAD branch forms the less intense South-Eastward Portugal Current (PC). The PC will eventually merge more to the South with the AzC. Both currents will then delimit the eastern Subtropical Gyre.

The region that includes the Bay of Biscay, delimited by the NAD, the AzC and the Eastern borders (Portuguese, Spanish, French and United-Kingdom coasts) can be split into three distinct areas: the abyssal plain, the continental slope, and the continental shelf.

2.2 North-Atlantic and Bay of Biscay Waters Description

Water masses are formed at the surface in precise regions of the Ocean. They are then transported to different regions and to different depths and tend to preserve in time their characteristics in potential temperature and salinity. Table 1 describes the water masses from the North-Atlantic Ocean found in the Bay of Biscay [1].

2.3 The abyssal plain

The general circulation in the first hundreds meters is characterized by the anti-cyclonic Portugal Current (PC). At a lower scale, essentially anti-cyclonic eddies are frequently observed with a typical diameter ranging from 50 to 100 km. The abyssal plain is separated from the continental shelf by the shelf-slope, along which a strong slope current develops showing strong seasonal and inter-annual variability.

2.4 The continental slope

The large scale meridional surface density gradient generates an Eastward flow. The consequent volume accumulation near the coast on the shelf creates a level gradient that generates a Northward geostrophic current along the shelf slope, thus separating the shelf

Table 1: Water masses in the North-eastern Atlantic Ocean.

Water masses	Depth (m)	T (°C)	S	σ (kg.m^{-3})
ENACW (sub-tropical branch)	< 300	> 12.5	> 35.75	< 27.05
ENACW (sub-polar branch)	< 400	$10.5 - 12.5$	$35.6 - 35.7$	$27.1 - 27.2$
ENACW (Bay of Biscay)	< 600	$10.5 - 11.5$	$35.6 - 35.6$	$27.2 - 27.3$
MW (surface core)	$400 - 700$	$11.8 - 12.2$	$35.8 - 35.9$	$27.2 - 27.3$
MW (upper core)	$700 - 900$	$10.5 - 13.5$	$35.8 - 36.8$	$27.4 - 27.7$
MW (lower core)	$1000 - 1500$	$9.5 - 12.5$	$35.8 - 37.5$	$27.7 - 27.9$
EASAIW	$500 - 1500$	$6.0 - 9.0$	$35.1 - 35.3$	$27.4 - 27.6$
LSW	$1500 - 3000$	$3.4 - 4.0$	$34.9 - 35.0$	$27.7 - 27.8$
LDW	> 3000	< 3.3	$34.9 - 35.0$	> 27.8

dynamics, from the deep Ocean's. The slope current is coupled with a downwelling motion that lowers the isopycnals. The slope current is highly baroclinic and its direction may inverse with depth.

The zonal wind is another driver of the circulation. During summer, the Azores anti-cyclone is centred on the North-Atlantic. On Europe's western coast, Northerly winds are predominant. This causes an offshore water transportation resulting in upwelling events and a diminution in intensity of the slope current. During winter, the Azores anti-cyclone moves southward, and thus the Westerly winds become predominant in Europe's western coast. The slope current is thus intensified and propagates northward penetrating into the Bay of Biscay as the Navidad current. Its width is around 40 km, its depth goes down to 200 m and typical currents reach 10 - 20 cms-1.

The Navidad current shows a very strong seasonal and inter-annual variability that seems to correlate well with the North-Atlantic Oscillation (NAO) index. Changing winds and bathymetry accidents, such as canyons, can easily cause this current to disperse and generate eddies called SWODDIES (Slope Water Oceanic eDDIES), because they trap warm and salty surface waters and transports them to the center of the Bay of Biscay.

2.5 The continental shelf

The Bay of Biscay comprises a large French continental shelf oriented in the North-South direction, and a narrower Spanish continental shelf oriented in the East-West directions. The French continental shelf size ranges from 300 km over the Armorican region, down to 50 km in the Aquitan region. The Spanish continental shelf is the narrowest, with only 30 to 40 km wide. The circulation over the shelf is highly influenced by physical

processes such as tide, wind and river discharges.

Tidal currents intensity depends largely on the water column depth: deeper water column will yield a less intense tidal current, whereas shallower water columns will yield more intense currents. This is a consequence of the momentum conservation principle. Also, refraction and other non-linear couplings may occur due to irregularities in the bathymetry. The tide-driven current intensity ranges from a few centimetres per second to nearly a meter per second (near Ushant). But in the southern part of the Bay of Biscay, velocities are nearly zero. Tide driven currents are more intense over the shelf, and the shear stress induced introduces strong vertical mixing between surface waters and bottom waters.

Internal waves are reputed to contribute to the general Ocean mixing and to the equilibrium of the thermohaline circulation [19]. The interaction of internal waves with topography can induce energy transfers, instability development and internal waves breaking [26].

The Ushant front (longitude bounded between 6°W and 4°W, and latitude bounded between 47.5ºN and 49ºN) is a result of the interaction between topography and tidal currents, which are very intense near Ushant [16]. In this shallow water area, the bottom friction homogenizes the water column and avoids the forming of a seasonal thermocline, whereas, westwards, the water column is deeper, and the bottom friction is not enough to homogenize, and a seasonal thermocline is formed. Thus, during summer, an intense horizontal density gradient is formed and is called the Ushant front. The front is dynamically unstable as wind and topography may interact with it. Near the coast, the tidal currents are less intense, and the seasonal thermocline appears, thus forming an internal front. The Ushant front is characterized by a 1 to 2 K / km thermal gradient, and the temperature difference between the cold water and the warm water can reach over 5 K.

Over the continental shelf, seasonal stratification is rather common. Tidal currents however, tend to homogenize the stratification and form complex hydrological structures, such as the Ushant front. The inter-annual stratification variability depends on the interaction of several processes such as the heat balance at the surface interface, the river plumes and the general circulation over the shelf [21].

2.6 In-situ data inventory

The available field and remote data inventory to validate the models results and confirm the current knowledge of hydrographic features consist of a climatology from IFREMER with 0.4º resolution and 261 layers covering the whole region of the bay of Biscay. Daily, weekly, monthly and yearly MODIS SST covering the whole region are also available. In-situ profiles of salinity and temperature of the Ushant region are available at the cross-sections of coordinates 46.5ºN, 5ºW to 47.6ºN, 3ºW and 46.3ºN, 4.4ºW to 47.1ºN, 2.4ºW, made respectively during the PELGAS campaign, 28-04-2004 to 23-05-2004, and during the EVHOE campaign, 29-10-2004 to 12-12-2004. Tidal stations data and buoys are also available and prepared for the bay of Biscay inter-comparison exercise, though the data

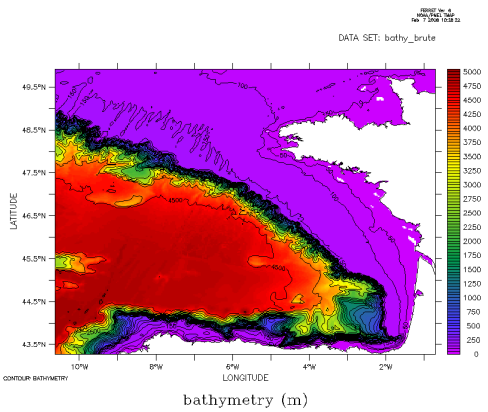

Figure 1: Original bathymetry used for the intercomparison.

was not used in this work.

3 MODELLING STRATEGY

3.1 The models and the forcing data

MOHID and NEMO-OPA are the numerical models used in this work, their description is presented in table 2 below.

MOHID encompasses a standard finite-volume approach of the Ocean Primitive Equations, using a generic combination of sigma and/or cartesian vertical coordinates with an ADI semi-implicit scheme for the horizontal advection-diffusion numerical schemes, as well as possessing a complete suite of modern and standard OBC, the MOHID model is comparable in its specifications to ROMS or NEMO-OPA [12, 23].

NEMO(Nucleus for European Modelling of the Ocean) is a state-of-the-art modeling framework for oceanographic research and operational oceanography. OPA is an Ocean Parallel model. NEMO is distributed under CeCILL license.

The bathymetry used for the intercomparison is from SHOM(Service Hydrographique et Océanographique de la Marine) and ETOPO5'(Electronic TOPOgraphic maps) and presents an initial resolution of 1´.

The Météo-France ALADDIN(Aire Limitée Adaptation Dynamique Développement International) model was used for atmospheric forcing with a 0.1º resolution and a 3 h timestep. Its data includes daily fields of surface atmospheric pressure, specific humidity at 2 m, air temperature at 2 m, zonal wind speed at 10 m, meridional wind speed at 10 m, zonal wind stress, meridional wind stress, precipitation, brut solar flux and IR flux.

The model MOG2D(2D gravity waves model) [14] provides fields for the M2, N2, K2, S2, K1, O1, P1, Q1 and M4 components of tide, whereas the PSY2V1 tide-free ocean basin solution, from Mercator-Océan, provides the salinity, temperature and current velocity fields with a 1/15º of horizontal resolution. Time-series of daily measurements of the main rivers Loire, Garonne and Adour were used to generate the land river run-off.

Table 2: Description of the models used in the intercomparison

	NEMO-OPA	MOHID
Free Surface	Time-spliting linear free surface	Time-coupled free surface, ADI semi-implicit [11]
Vertical coordinate	Cartesian + partial-step (the bottom layer adapts itself to the bathymetry), 49 levels	Cartesian + partial-step cells (minimum is 5% of the layer thickness), 43 levels
Advection tracer	QUICKEST + ULTIMATE [13]	TVD scheme (explicit in horizontal and implicit in vertical)
Horizontal Diffusion	constant	constant
Corrections to advection scheme	Preserves the energy and the enstrophy	-
Corrections to turbulent diffusion scheme	Biharmonic 5.10^8 $m^4\,s^{-1}$	Biharmonic 10^9 $m^4\,s^{-1}$[6]
Vertical turbulent diffusion scheme	[2]	GOTM model [5]
Surface forcing	BULK formula [10]	BULK formula [9]
Barotropic timestep	4s	90 s
Baroclinic timestep	240s	90 s

Table 3: Bathymetry filtering method for NEMO-OPA and MOHID

Model	Bathymetry processing	Reason
NEMO-OPA	Minimum depth of 5.75 m	To avoid having too few layers in shallow water areas.
MOHID	Filtering high gradient areas.	MOHID runs a tool that checks every cell of the bottom layer and assures that a minimum thickness ratio with adjacent cells is guaranteed.

3.2 Numerical models setup

Both the NEMO-OPA and MOHID models solve the Ocean primitive equations, containing a set of 5 differential equations, the u and v component of the momentum equations, the continuity equation (to calculate the w component of momentum and the water elevation), and the advection-diffusion of the salinity and temperature tracers. The momentum and tracer equations possess advection, diffusion and sources and sink terms [3]. Typically, the source and sink terms regulate fluxes at the surface-sea or at the land-sea interface, such as heat fluxes and freshwater discharges, respectively. Advective and diffusive processes, on the other hand, are handled at the lateral boundaries by OBC or land-water null-fluxes conditions. The advection numerical schemes, the vertical coordinate type, the turbulent diffusion scheme and the atmospheric forcing bulk formulae of both models are described in table 2.

The regular horizontal grid has a resolution of 3 km (1/36°), which is slightly finer than 2:1 relatively to the PSY2V1 ocean forcing solution, which is considered an adequate ratio for downscaling or for offline nesting [20].

For both models, the bathymetric data is interpolated linearly in the horizontal grid, though each model may or may not add some smoothing filter, described in table 3, in order to eliminate numerical stability problems typically created by problematic cells near the bottom.

Besides the bathymetry, the variables u, v, the level, η, S and T need to be initialized. S and T are directly interpolated from the PSY2V1 reference solution in both models. u, v and η are nullified in NEMO-OPA. In MOHID, u, v and η are initialized using the

Table 4: Initialization methods used in NEMO-OPA and in MOHID.

Model	initialization
NEMO-OPA	S and T are interpolated to the PSY2V1 field. Null velocity field and null water elevation
MOHID	Horizontal interpolation and vertical re-interpolation. S and T are interpolated to the PSY2V1 field. The velocity fields and the water elevation follow a geostrophic initialization.

geostrophic equilibrium with density [8]. The interest in the geostrophic initialization, compared to the null-velocity initialization, is the shorter spin-up time to reach a fully developed kinetic energy field. More details regarding initialization are shown in table 4.

The river run-offs are modeled as a freshwater discharge (source term in the tracer equation) in the nearest cell of the eastuary's mouth.

The used algorithms for the OBC are displayed in table 5. They mostly consider the Flather radiation condition to both impose the tide signal and to radiate outgoing gravity waves, added of a flow relaxation scheme with a sponge layer [17] to absorb all other outgoing perturbations (namely momentum and internal waves) as well as to impose incoming momentum and density gradients coming from the PSY2V1 thermohaline reference solution.

The NEMO-OPA simulation lasted roughly 3 days on a 12 CPUs Fujtsu/Siemens cluster. Each CPU is an AMD Opteron dual-core 64 bits between 2 and 2.2 GHz.

The MOHID simulation lasted around 37 days (using only a single core) Intel Core 2 Extreme X9650 3 GHz, 8 GB RAM.

4 RESULTS VALIDATION, COMPARISON AND ANALYSIS

A heat and salt balance was performed by interpolating/extrapoling all models results, the reference solution and the climatology to a reference grid with the same vertical Cartesian discretization, and then by integrating over the whole region, as seen in figure 2. The PSY2V1 reference solution thermal fluctuation is quite different from the climatology, whereas, both models NEMO-OPA and MOHID are in very good agreement, equally, with the climatology. This difference is explained by the fact that the atmospheric forcing of the models is different than that of the reference solution. All models, except MOHID, have very different ending values for the salt balance, including the PSY2V1 reference solution.

Table 5: Numerical OBC schemes.

	NEMO-OPA	MOHID [12]
Barotropic OBC	[7] (η, u, v)	[7]
Baroclinic OBC	specified at the boundary	flow relaxation scheme u, v [18] + viscosity sponge [6]
Tracer OBC	specified at the boundary	flow relaxation scheme S, T [18]
Relaxation zone	15 grid-cells wide in space and one day duration (for T and S only)	30 grid-cells wide in space and one third of day duration for u, v, S and T. Exponencial decay in space directed away from the relaxation zone.
Relaxation period	daily	daily

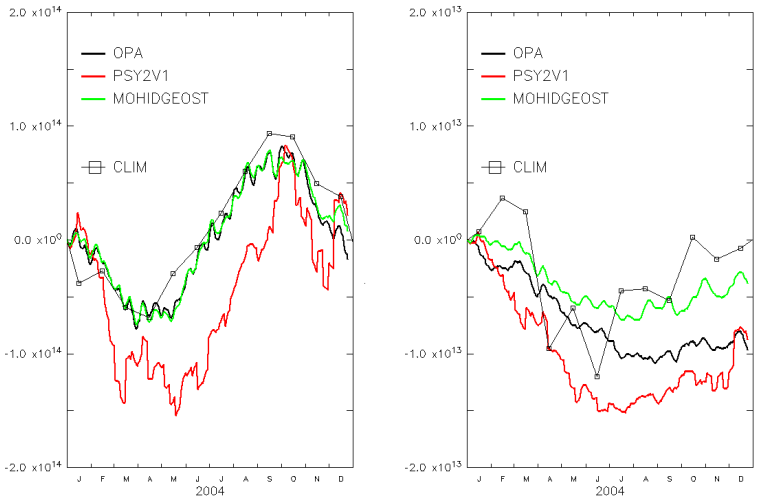

Figure 2: Thermal (left panel) and haline (right panel) balance normalized to the initial value obtained for each model. The climatology is also represented.

While MOHID haline balance follows better the climatology and tends to diverge from the reference solution, the NEMO-OPA is in phase and follows better the reference solution.

The overall annual mean circulation is presented in figure 3 for the PSY2V1, the NEMO-OPA and the MOHID solutions.

The globally cyclonic PSY2V1 circulation of the abyssal plain, which contours two anti-cyclonic eddies, presents an excessively intense slope current (which is an already known error of this model). On the shelf however, circulation is overall anti-cyclonic. The mean circulation of the other models, although preserving the same overall cyclonic/anti-cyclonic feature, has qualitatively and quantitatively very distinct traits, namely on the positioning and the intensity of each recirculation pattern. Lack of current data forbids assessing which model is best. However, the efficiency of the numerical schemes at the OB can be discussed for each model.

As the models evolve and the fields diverge further and further away from the reference solution, due to better atmospheric forcings and better resolution, over-relaxation of salinity and temperature tends to create an artificial front all along the OB that will tend to generate spurious geostrophic residual flow. This residual geostrophic flow will store available potential energy (APE) and enstrophy generated inside the domain, while isolating wave-like information from propagating out-ward and in-ward the domain, thus also deprecating the interior solution away from the OB. Thus the relaxation decay-times are a critical aspect that must be parameterized for each model and each reference solution. They are ill-defined when a geostrophic flow occurs at the OB and when permanent fronts are created after a long enough period of simulation. MOHID was over-relaxed

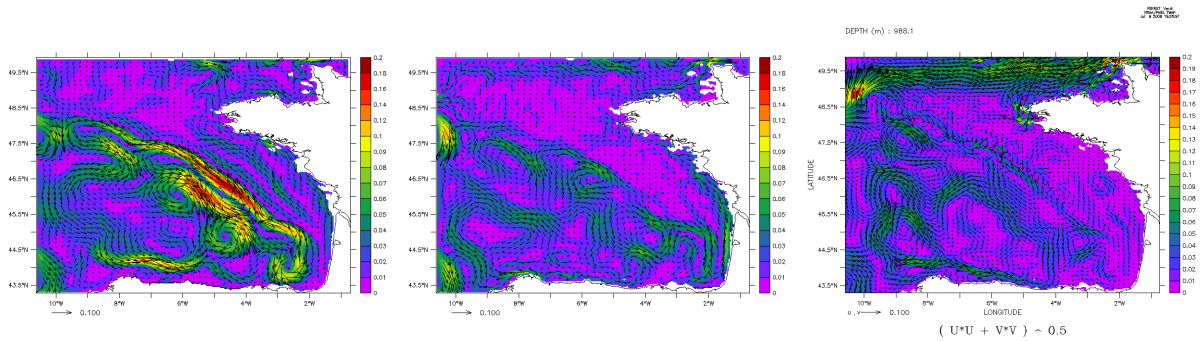

Figure 3: Yearly average tide-removed KE and velocity fields during 2004 at 15 m depth. Left panel, PSY2V1. Middle panel, NEMO-OPA. Right panel, MOHID.

compared to NEMO-OPA by a three-fold factor at the OB, and also used a wider relaxation zone. However NEMO-OPA uses a constant decay-time all along its relaxation zone, while MOHID uses an exponentially growing relaxation time directed away from the OB.

The June 15th MODIS satellite SST shows a good cloud-free coverage of the area while evidencing clear frontal structures. The comparisons of this satellite image with the models are presented in figure 4 where the average bias with MODIS was removed.

The lower temperatures on the north shelf (which includes the Ushant front) are highly correlated with strong tidal currents and indicate an area where tidal mixing is maximal. Along the northern part of the continental slope, a thermal front is formed induced by internal waves mixing. The rest of the French continental shelf presents warmer waters and upwelling between the Landes and the mouth of Gironde's estuary. A large upwelling seems to be occurring along the Spanish coast in the models, and probably in the Satellite data despite the cloud cover.

The NEMO-OPA model reproduces appropriately the thermal structures described above. The MOHID results seem to evidence a less variability than could be expected. This may be due to the coarse vertical discretization at the surface. Also, the model is relaxing too strongly to the reference PSY2V1 solution at the western OB. MOHID relaxation time is around 30000 s while, NEMO-OPA are around 90 000 s (1 day).

The Ushant front can be well described by satellite imagery even though it is a near-shore process. Cloud-free events were spotted by MODIS near the area on on July 6th (figure 5) and were compared with the models with and without bias towards MODIS. Also, the temperature zonal section at 48.15°N (bounded by 6°W to 4°W) is compared with the literature in the rightmost panel of figure 5 for the same date.

Figure 5 represent the Ushant front, composed of two cold lobes. Both models represent them correctly qualitatively. However, due to the 8 m thick superficial layer, MOHID results are too cold. The vertical sections are consistent with the scientific description found in the literature for both models.

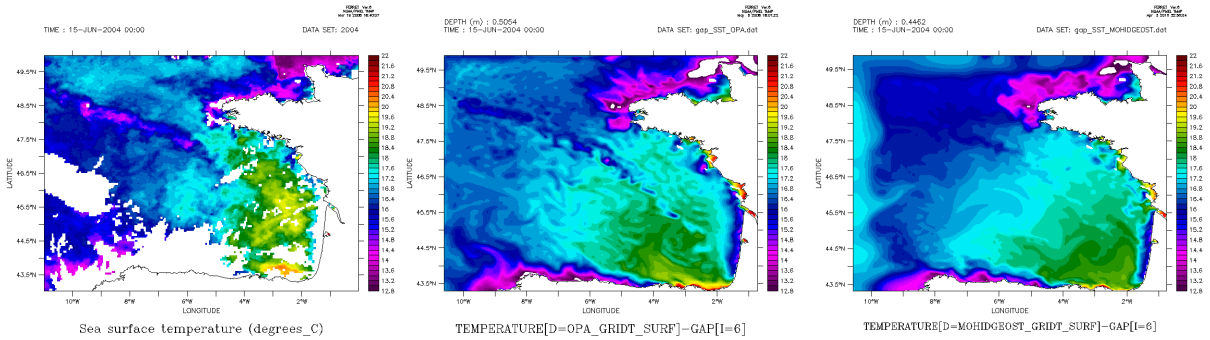

Figure 4: SST MODIS comparison with the models NEMO-OPA and MOHID for the June 15th. Top-left panel, MODIS image. Top-right panel, NEMO-OPA model. Bottom panel, MOHID model. The SST average difference between the models and MODIS was removed.

The offshore distance of the front is an important characteristic of the region. Thus, Hovmuller diagrams along the section SST were created for each model and for the satellite data (figure 6). To be able to compare the diagrams between model and satellite, the minimum SST was removed from each diagram. Figure 7 represents the time evolution of temperature minimum in the left panel, in order to representing the temperature evolution of the front. Right panel of figure 7 represents the time evolution of the position of the temperature minimum, in order to represent the evolution of the front's position.

Observations on the left-panel of figure 6 show that the minimum of temperature is leaned on the coast during the winter period (January to April and November to December), and is situated around the 5.1°W during the summer period (May to October). During this period, the temperature differences clearly show the presence of a front. During the April and October months, we observe a transient period between the winter/summer states that is characterized by a homogeneous SST.

The results obtained with both models are very consistent showing clearly the seasonal migration of the front. The temperature gradient maxima, however, during summer are too weak for NEMO-OPA, and too strong for MOHID; whereas during winter, they are far too strong for MOHID, and slightly too strong for NEMO-OPA. Finally, the front in MOHID is too thin during winter.

The left panel of figure 7 shows that, again, the MOHID SST is cooler than the NEMO-OPA SST, probably because of its thick over-mixed superficial layer. However both models results seem to correlate very well with the MODIS data with what looks like an acceptable RMSE. The right panel of figure 7 shows the evolution of the front position, represented by the SST minimum, between two states, winter and summer. Both NEMO-OPA and MOHID evolve in phase with the obersvations between the winter/summer states. MOHID however performs somewhat better during the transient months of April and October.

Figure 8 shows that this cold water body is present in the extrapolated/interpolated climatology (top right). The model results (bottom panels) show the presence of the cold water body. The MOHID solution shows a clearer folding of the isopycnics than

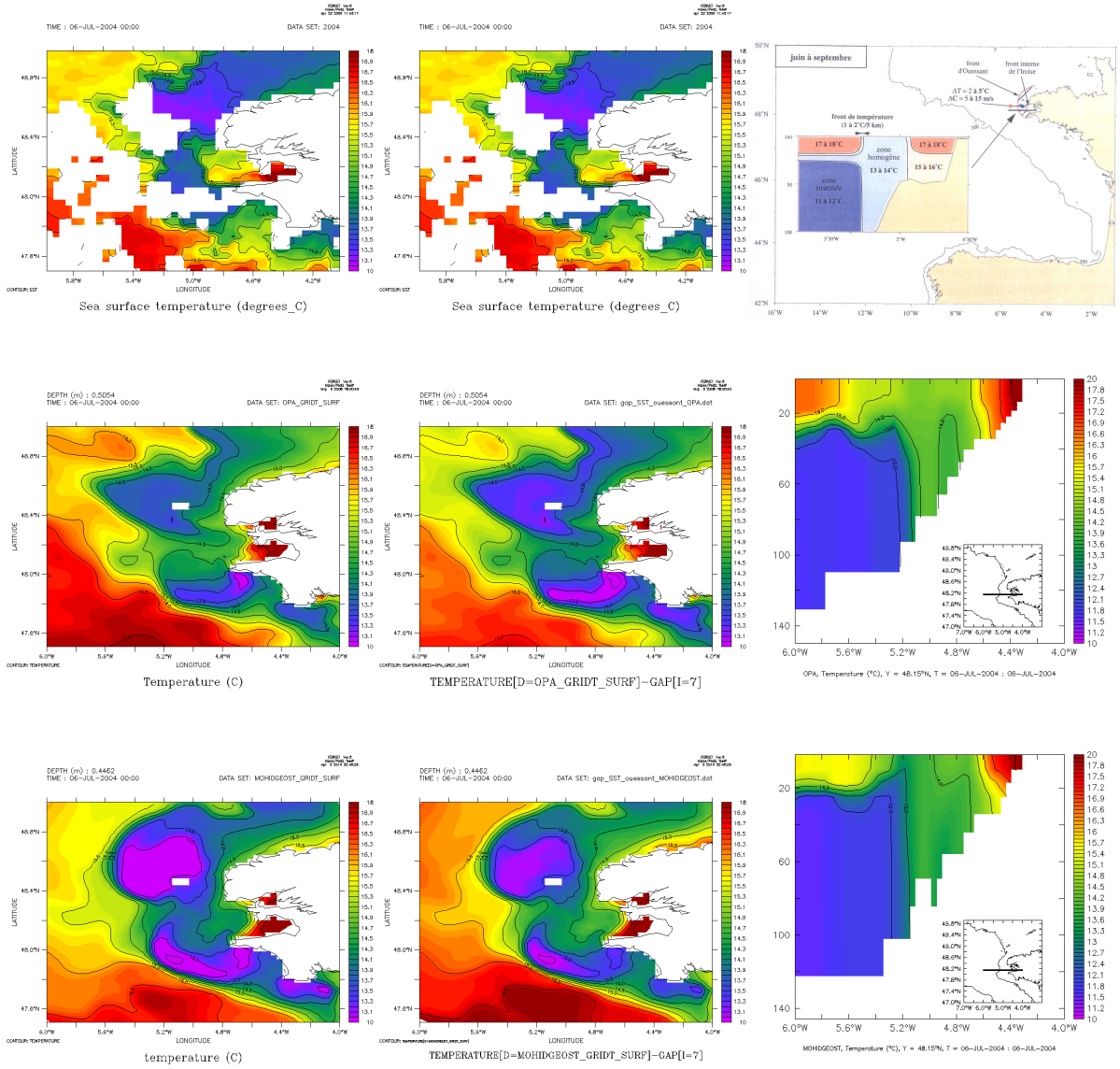

Figure 5: July 6th event in the Ushant area. Top panels: MODIS and litterature data. Middle panels: NEMO-OPA results. Bottom panels: MOHID results. Left panels: SST. Center panels: SST with the average difference with MODIS removed. Right panels: Cross-section at 48.2ºN, between 6ºW and 4ºW.

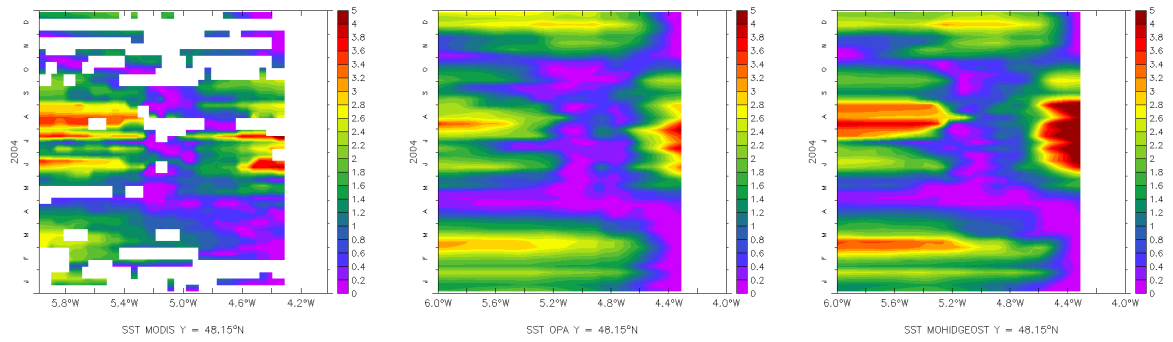

Figure 6: Hovmuller diagrams of the temperature offset relatively to the minimal temperature found along the Ushant section (6°W to 4°W at 48.15°N), of the MODIS SST (leftmost panels) and the models SST (NEMO-OPA in the middle panel and MOHID in the rightmost panel).

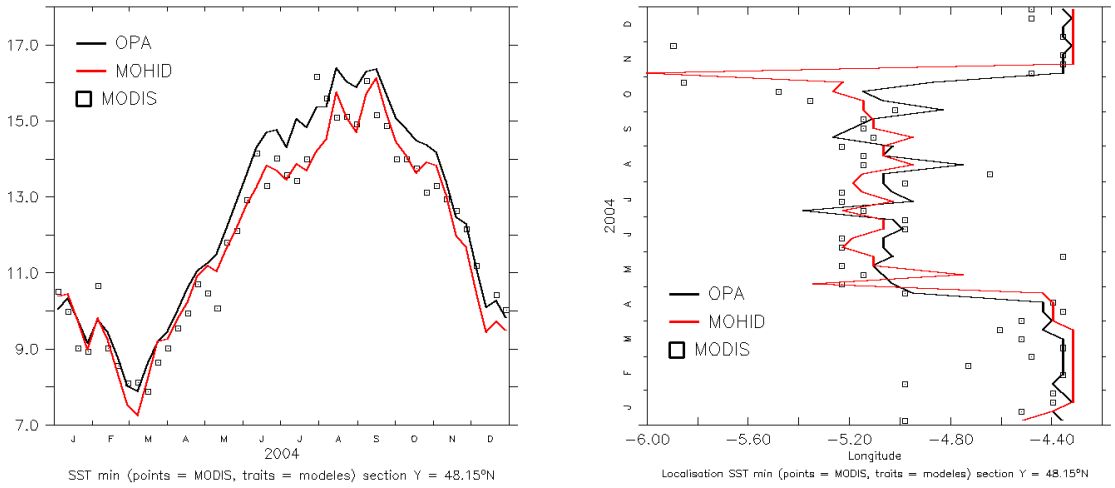

Figure 7: left panel: Minimum SST evolution of the Ushant section section (6°W to 4°W at 48.15°N). Right panel: Position evolution of the SST minimum in the Ushant section (right panel).

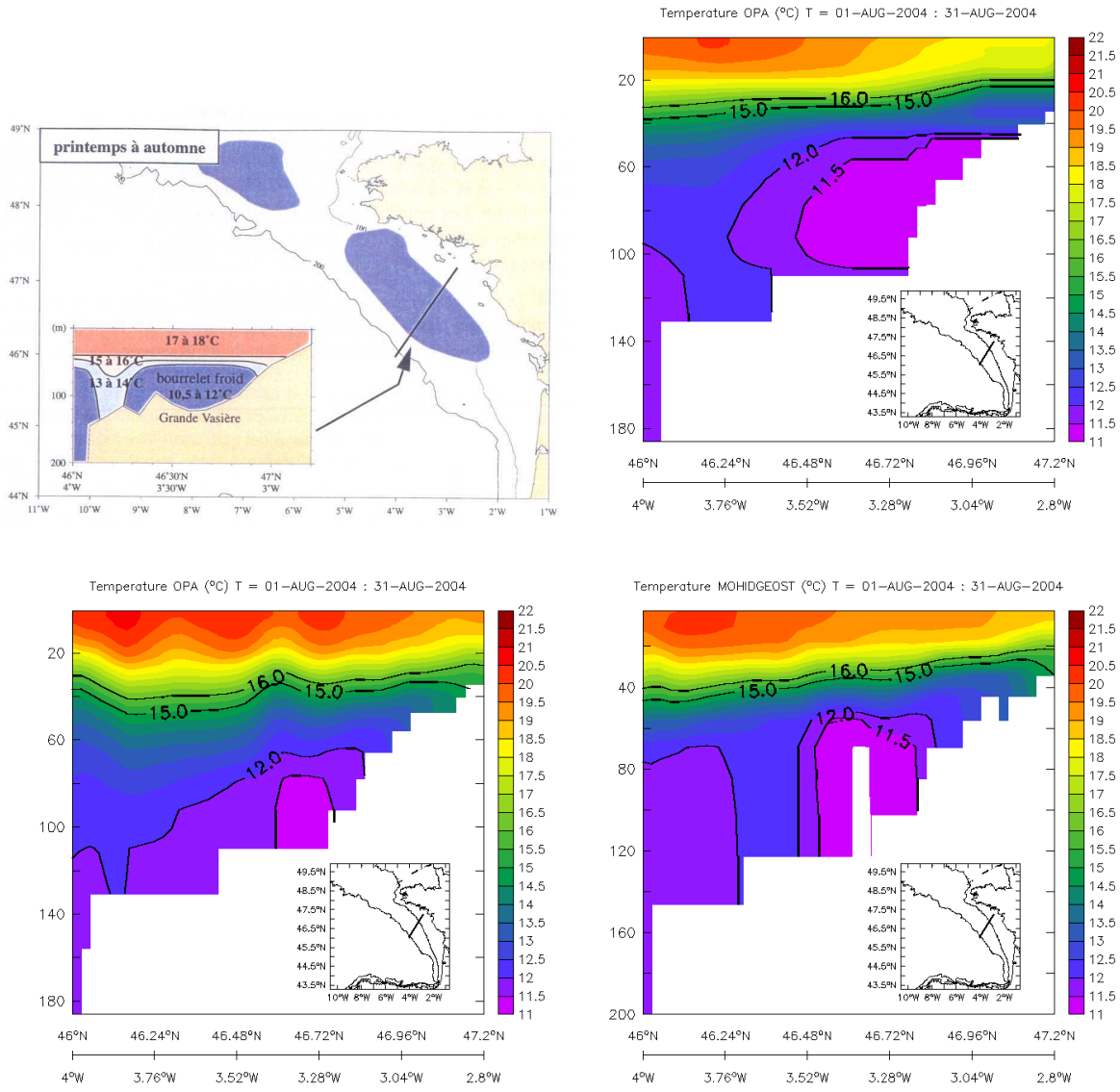

Figure 8: Cross-section from 46°N, 4°W to 47.2°N, 2.8°W of the la Vasière cold water mass during August. Temperature comparison between literature (top left), climatology (top right) and the models (bottom).

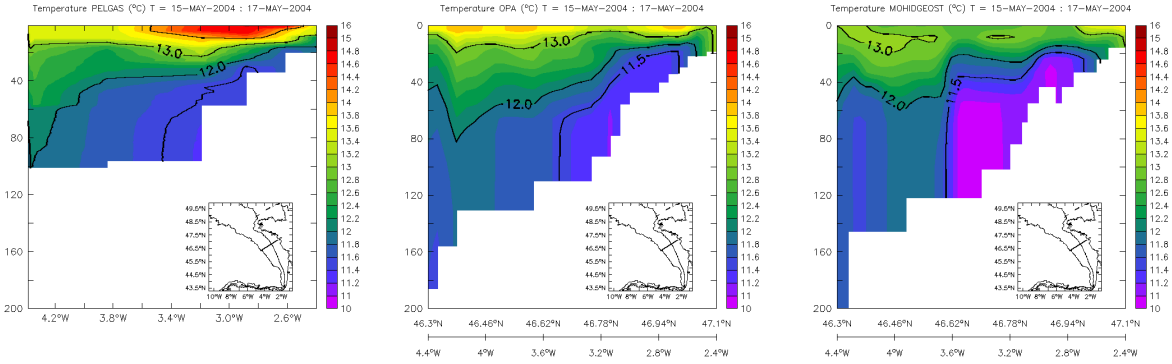

Figure 9: Cross-section from 46.5°N, 5°W to 47.6°N, 3°W of the la Vasière cold water mass during PELGAS campaign, from the 15th to the 17th of May. Temperature comparison between PELGAS (left), NEMO-OPA (middle) and MOHID (right).

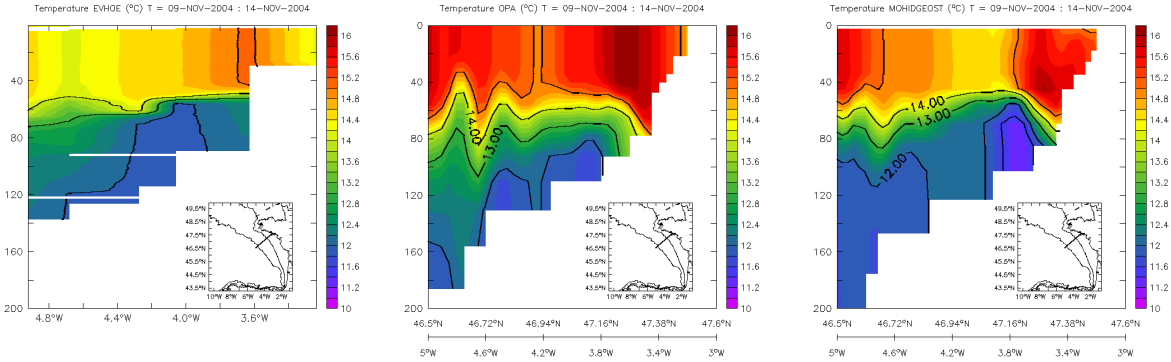

Figure 10: Cross-section from 46.3°N, 4.4°W to 47.1°N, 2.4°W of the la Vasière cold water mass during EVHOE campaign, from the 9th to the 14th of November. Temperature comparison between EVHOE (left), NEMO-OPA (middle) and MOHID (right).

the NEMO-OPA solution. The freshwater plume from the river run-offs intensifies the stratification at the surface and inhibit the vertical mixing of the cold water body, thus it preserves its form and enhances the isopycnic folding.

Sections were built from data from the PELGAS (figure 9) and EVHOE (figure 10) cruises. Both sections show the presence of a cold water body. In the PELGAS case (figure 9), both NEMO-OPA and MOHID reproduce quite well the cold water body, with a clear sign of the isopycnic folding. In the EVHOE case (figure 10), MOHID is qualitatively in better agreement than NEMO-OPA, although both models solutions are warmer than the measurements.

5 CONCLUSION

As a general conclusion relative to the intercomparison of models, NEMO-OPA tends to follow more closely the reference PSY2V1 solution than MOHID. This should be expected since both PSY2V1 and NEMO-OPA share the same source-code. MOHID is generally colder at the surface because of its thicker 8 m depth surface layer that over mixes the surface water. Otherwise, both models seem to perform quite well, when compared against exhibited in-situ data. On the downside, MOHID exhibits a too stiff relaxation at the western OB which may generate a spurious residual geostrophic current.

For the purpose of downscaling techniques applied to OGCM, the techniques used, independently, by both teams IST and Mercator-Océan, proved to be quite similar, differing only in the parameterization terms (such as the relaxation times near the OB, which would influence the quality of the results), and in the numerical schemes. MOHID uses a slightly different initialization technique, as it computes the geostrophic currents from the initial density field. These downscaling techniques, designed to be used with an OGCM in offline mode, seem to evidence the feasibility of successfully implementing operational systems that can forecast the circulation of regions nested in the OGCM domain, while adding more physics, such as tide, and freshwater river runoffs and improving the existing physics, such as the atmospheric forcing. It can be expected to see the implementation of operational regional circulation systems in the years to come; using as offline OGCM the Mercator-Océan forecast solution.

REFERENCES

[1] Ambar, I. A shallow core of Mediterranean water off western Portugal. *Deep-Sea Research 30*, 6A (1983), 677–680.

[2] Blanke, B., and Delecluse, P. Low frequency variability of the tropical Atlantic ocean simulated by a general circulation model with mixed layer physics. *J. Phys. Oceanogr 23*, 8 (1993), 1736–1753.

[3] Bryan, K. A numerical method for the study of the circulation of the world ocean. 347–376.

[4] Canas, A., Santos, A. D., and Leitão, P. C. Effect of large scale atmospheric pressure changes on water level in the tagus estuary. *Journal of Coastal Research SI56* (2009), 1627–1631.

[5] Canuto, V. M., Howard, A., Cheng, Y., and Dubovikov, M. S. Ocean turbulence. part i: One-point closure model-momentum and heat vertical diffusivities. *Journal of Physical Oceanography 31*, 6 (June 2001), 1413–1426.

[6] Delhez, É., and Deleersnijder, É. Overshootings and spurious oscillations caused by biharmonic mixing. *Ocean Modelling 17*, 3 (2007), 183–198.

[7] Flather, R. A. A tidal model of the northwest European continental shelf. *Mem. Soc. R. Sci. Liege 10*, 6 (1976), 141–164.

[8] Gill, A. E. *Atmosphere-ocean dynamics*. Academic Press New York, 1982.

[9] Kraus, E. B., and Businger, J. A. *Atmosphere-ocean interaction*. Oxford University Press, USA, 1994.

[10] Large, W. G., McWilliams, J. C., and Doney, S. C. Oceanic vertical mixing: A review and a model with a vertical K-profile boundary layer parameterization. *Rev. Geophys 32*, 4 (1994), 363–403.

[11] Leendertse, J. J., and Liu, S. K. A three-dimensional turbulent energy model for nonhomogeneous estuaries and coastal sea systems. In *Hydrodynamics of estuaries and fjords, Volume 23: Proceedings of the 9th International Liège Colloquium on Ocean Hydrodynamics* (1977), J. C. J. Nihoul, Ed., vol. 23, Elsevier Science, pp. 387–406.

[12] Leitão, P., Coelho, H., Santos, A., and Neves, R. Modelling the main features of the algarve coastal circulation during july 2004: A downscaling approach. *Journal of Atmospheric & Ocean Science 10*, 4 (2005), 421–462.

[13] Leonard, B. P. The ULTIMATE conservative difference scheme applied to unsteady one-dimensional advection. *Computer methods in applied mechanics and engineering 88*, 1 (1991), 17–74.

[14] Lyard, F., Lefevre, F., Letellier, T., and Francis, O. Modelling the global ocean tides: modern insights from fes2004. *Ocean Dynamics 56*, 5-6 (December 2006), 394–415.

[15] Malhadas, M., Neves, R., Leitão, P., and Silva, A. Influence of tide and waves on water renewal in Óbidos lagoon, portugal. *Ocean Dynamics 60*, 1 (February 2010), 41–55.

[16] Mariette, V., and Le Cann, B. Simulation of the formation of Ushant thermal front. *Continental Shelf Research 4* (1985), 637–660.

[17] Marsaleix, P., Ulses, C., Pairaud, I., Herrmann, M. J., Floor, J. W., Estournel, C., and Auclair, F. Open boundary conditions for internal gravity wave modelling using polarization relations. *Ocean Modelling 29*, 1 (2009), 27–42.

[18] Martinsen, E. A., and Engedahl, H. Implementation and testing of a lateral boundary scheme as an open boundary condition in a barotropic ocean model. *Coastal engineering 11*, 5-6 (1987), 603–627.

[19] Munk, W., and Wunsch, C. Abyssal recipes II: energetics of tidal and wind mixing. *Deep-Sea Research Part I 45*, 12 (1998), 1977–2010.

[20] Penven, P., Debreu, L., Marchesiello, P., and Mcwilliams, J. C. Evaluation and application of the ROMS 1-way embedding procedure to the central California upwelling system. *Ocean Modelling 12* (2006), 157–187.

[21] Puillat, I., Lazure, P., Jégou, A. M., Lampert, L., and Miller, P. I. Hydrographical variability on the French continental shelf in the Bay of Biscay, during the 1990s. *Continental shelf research 24*, 10 (2004), 1143–1163.

[22] Riflet, G., Juliano, M., Fernandes, L., Leitão, P. C., and Neves, R. Operational ocean forecasting of the portuguese waters. *Mercator-Océan Quarterly Newsletter*, #30 (July 2008), 20–32.

[23] Riflet, G., Leitão, P. C., Fernandes, R., and Neves, R. J. J. A simple pre-operational model for the portuguese coast. In *CMNE/CILAMCE 2007 porto, 13 a 15 de Junho* (June 2007), FEUP.

[24] Tartinville, B., Deleersnijder, E., Lazure, P., Proctor, R., Ruddick, K. G., and Uittenbogaard, R. E. A coastal ocean model intercomparison study for a three-dimensional idealised test case. *Applied Mathematical Modelling 22*, 3 (JanuarySeptemberSeptemberAugust/March 1998), 165–182.

[25] Vaz, N., Dias, J. a. M., and Leitão, P. C. Three-dimensional modelling of a tidal channel: The espinheiro channel (portugal). *Continental Shelf Research 29*, 1 (January 2009), 29–41.

[26] Wunsch, C., and Ferrari, R. Vertical mixing, energy, and the general circulation of the oceans. *Annual Review of Fluid Mechanics 36* (2004), 281–314.